mRNA bound to the 30S subunit is a HigB toxin substrate

MARC A. SCHURECK, TATSUYA MAEHIGASHI, STACEY J. MILES, JHOMAR MARQUEZ, and CHRISTINE M. DUNHAM

Department of Biochemistry, Emory University School of Medicine, Atlanta, Georgia 30322, USA

ABSTRACT

Activation of bacterial toxins during stress results in cleavage of mRNAs in the context of the ribosome. These toxins are thought to function as global translational inhibitors yet recent studies suggest each may have distinct mRNA specificities that result in selective translation for bacterial survival. Here we demonstrate that mRNA in the context of a bacterial 30S subunit is sufficient for ribosome-dependent toxin HigB endonucleolytic activity, suggesting that HigB interferes with the initiation step of translation. We determined the X-ray crystal structure of HigB bound to the 30S, revealing that two solvent-exposed clusters of HigB basic residues directly interact with 30S 16S rRNA helices 18, 30, and 31. We further show that these HigB residues are essential for ribosome recognition and function. Comparison with other ribosome-dependent toxins RelE and YoeB reveals that each interacts with similar features of the 30S aminoacyl (A) site yet does so through presentation of diverse structural motifs.

Keywords: toxin–antitoxin modules; stringent response; RNase; ribosome; protein synthesis; mRNA

INTRODUCTION

Restriction of energy-consuming processes during stress is required to conserve metabolites and maintain basal levels of growth. The bacterial stress or stringent response detects diminishing nutrients and promotes a cascade of events to limit growth and activate specific gene expression to survive new environmental conditions (Boutte and Crosson 2013). Toxin–antitoxin gene pairs are part of the stringent response whereby antitoxin degradation releases toxin proteins to aid in growth limitation, biofilm, and persister formation (Yamaguchi and Inouye 2011; Maisonneuve and Gerdes 2014). Most bacteria contain multiple toxin–antitoxin operons and in some cases, specific toxin–antitoxin families have a greatly increased number of members leading to a diverse range of toxin targets (Pandey and Gerdes 2005; Yamaguchi and Inouye 2011).

There are five classes of toxin–antitoxin systems with the type II protein–protein family being the most abundant (Gerdes et al. 2005; Maisonneuve and Gerdes 2014). During nonstress conditions, the toxin–antitoxin complex binds to upstream DNA operator regions to inhibit transcription and limit their expression (Loris and Garcia-Pino 2014). Stress triggers antitoxin degradation by AAA+ ATPase proteases Lon, ClpAP, and ClpXP resulting in transcriptional derepression at the toxin–antitoxin operon and inhibition of replication and translation by the free toxin (Gerdes et al. 2005; Maisonneuve and Gerdes 2014). A majority of type II toxins are RNases that cleave tRNAs, rRNAs, and mRNAs, either free or specifically bound to the ribosome. It is unclear why certain toxin RNases require ribosome-bound mRNA when the cleavage of free mRNA would be sufficient for the inhibition of translation. This requirement may suggest a specialized mechanism that facilitates a defined translational response to a specific stress.

E. coli K12 contains at least 36 proposed chromosomally encoded, toxin–antitoxin operons with at least five that require the ribosome to cleave mRNA (Yamaguchi and Inouye 2011). The RelE, YoeB, YafQ, and HigB ribosome-dependent toxins cleave at a preferred mRNA sequence at positions along the entire transcript in the ribosomal aminoacyl (A) site on the 30S subunit. Since the mRNA is bound to the ribosome, cleavage along the entire mRNA suggests that ribosome-dependent toxins can target the three stages of the protein synthesis cycle—initiation, elongation, and termination. *E. coli* RelE and YoeB cleave both sense and stop codons (Pedersen et al. 2003; Christensen et al. 2004; Christensen-Dalsgaard and Gerdes 2008; Zhang and Inouye 2009), whereas *E. coli* YafQ and *Proteus vulgaris* HigB cleave at a single AAA lysine codon and adenosine-rich codons, respectively (Hurley and Woychik 2009; Prysak et al. 2009).

Corresponding author: christine.m.dunham@emory.edu

Article published online ahead of print. Article and publication date are at http://www.rnajournal.org/cgi/doi/10.1261/rna.056218.116.

Interestingly, the AAA lysine codon, preferentially targeted by YafQ and HigB toxins, is the most common codon to directly follow the AUG start codon in *Proteus mirabilis* and *E. coli* K12 (Sato et al. 2001; Hurley and Woychik 2009). This observation suggests that some ribosome-dependent toxins may target an initiation-competent ribosomal complex, that is, the small 30S subunit containing mRNA and initiator $tRNA^{fMet}$, expanding the number of ribosomal states that are potential toxin targets.

During translation, ribosome-dependent toxins compete with EF-Tu•tRNA•GTP ternary complexes and translation factors including initiation factor 1 (IF1) and release factors 1 and 2 (RF1 and RF2) for the empty, or non-tRNA bound, A site. Recently it was shown that the YafQ toxin has a comparable affinity for the ribosomal A site as tRNAs and translation factors (Maehigashi et al. 2015). However, since toxin–antitoxin complexes are expressed at extremely low levels under both nonstress and stress conditions (Overgaard et al. 2008; Li et al. 2014), one important question is, how do these toxins gain access to the A site to cleave mRNAs when they are low abundance and have comparable A-site affinities as translation factors and tRNAs?

Here we address one aspect of this question with the *P. vulgaris* host inhibitor of growth B (HigB) toxin, a ribosome-dependent endonuclease initially discovered on a kanamycin-resistance Rts1 plasmid associated with *Proteus vulgaris* (Tian et al. 1996). HigB cleaves adenosine-rich codon sequences and the AAA lysine codon is a primary mRNA target sequence (Hurley and Woychik 2009). Our results show that HigB cleaves mRNA programmed on the 30S initiation-competent complex. Moreover, we report a 3.6 Å X-ray crystal structure of HigB bound to the 30S, identify two clusters of basic residues that interact with 16S rRNA helices, and confirm their importance using mutagenesis and bacterial growth assays. Our results demonstrate that HigB, like RelE (Pedersen et al. 2003), is active on the 30S subunit and suggest that the initiation state, in addition to elongation and termination states, can be targeted by ribosome-dependent toxins.

RESULTS

HigB toxin can target the initiation step of translation

HigB cleaves multiple codon sequences with the AAA lysine codon being a major HigB target as shown by primer extension analysis (Hurley and Woychik 2009). Moreover in *Proteus mirabilis* and *E. coli* K12, the AAA lysine codon is the most common codon at the second position after the AUG start codon (Sato et al. 2001; Hurley and Woychik 2009). These observations suggest that the HigB endonuclease may target ribosomes during both initiation and elongation. We previously demonstrated that HigB recognizes a 70S elongation complex with the ribosome being essential for HigB-mediated mRNA cleavage (Schureck et al. 2015). However, whether HigB is active in cleaving mRNA on a 30S subunit is unknown.

To test whether HigB cleaves mRNAs bound to a 30S initiation-competent complex, we first programmed *E. coli* 30S subunits with a 25-nucleotide (nt) mRNA containing a strong Shine–Dalgarno sequence (AGGAGG) optimally spaced preceding an AUG start codon in the P site, and an AAA lysine codon in the A site (Fig. 1A). Next, we added 2.5-fold molar excess of *E. coli* $tRNA^{fMet}$ to bind in the P site. In the absence of the 30S, HigB is unable to cleave mRNA, demonstrating that HigB requires the ribosome for activity (Fig. 1B; lane 4). Additionally, incubation of 30S subunits with mRNA and $tRNA^{fMet}$ in the absence of HigB confirms the lack of contaminating RNase activity in these components (Fig. 1B; lane 5). Incubation of the 30S initiation-competent complex with HigB results in mRNA cleavage over a 60-min time course (Fig. 1B; lanes 6–11). HigB likely cleaves the mRNA transcript between the second and third A-site nucleotides yielding a 20-nt product containing a 2′–3′ cyclic phosphate or a 3′-phosphate (Fig. 1B; open arrow). The presence of a 3′-end phosphate after cleavage, as observed for RelE, YoeB, and YafQ toxins (Neubauer et al. 2009; Feng et al. 2013; Maehigashi et al. 2015), results in faster migration in the gel and the appearance of an apparent ~19-nt fragment. Although HigB was proposed to interact with the 50S subunit (Hurley and Woychik 2009), these results demonstrate that the 50S is not required for HigB-mediated mRNA cleavage.

Structural basis of HigB toxin recognition of the 30S subunit

To reveal the structural basis for HigB recognition of the ribosomal A site in the context of the 30S, we solved the 3.6 Å X-ray crystal structure of HigB bound to the *Thermus thermophilus (Tth)* 30S (Table 1; Fig. 2). Crystals of the *Tth* 30S subunit only grow in the *apo* form (Wimberly et al. 2000). In this

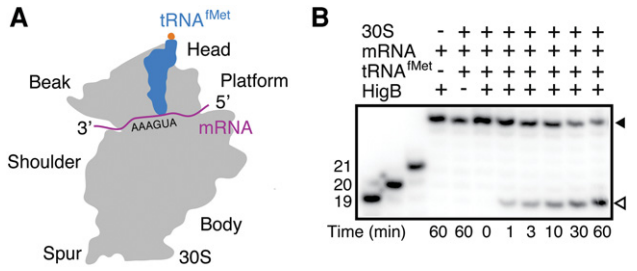

FIGURE 1. HigB cleaves mRNA bound to the 30S subunit. (*A*) Schematic of in vitro cleavage assays performed on the *E. coli* 30S ribosomal subunit with 30S domains labeled. (*B*) *E. coli* 30S was programmed with ^{32}P-labeled 25-mer mRNA containing an A-site 5′-AAA-3′ lysine codon, P-site $tRNA^{fMet}$, and HigB toxin, and mRNA cleavage was monitored over 60 min. Solid arrow indicates uncleaved mRNA, open arrow indicates the cleaved mRNA product, and 19-mer, 20-mer, and 21-mer standards are shown to the *left*.

TABLE 1. Crystallography statistics for the 30S-HigB structure

Data collection	
Space group	P 4_1 2_1 2
Cell dimensions	
a, *b*, *c* (Å)	402.6, 402.6, 176.0
α, β, γ (°)	90, 90, 90
Resolution (Å)	50–3.60 (3.73–3.60)[a]
R_{meas} (%)	11.9 (72.2)
R_{pim} (%)[b]	6.7 (40.8)
$CC_{1/2}$	0.997 (0.692)
I/σ	9.8 (1.8)
Completeness (%)	98.6 (99.6)
Redundancy	3.0 (3.0)
Refinement	
Resolution (Å)	50–3.60
Total reflections	491,888 (39,209)
Unique reflections	163,739 (12,894)
R_{work}/R_{free}	0.214 (0.314)/0.239 (0.352)
No. atoms	52,640
Protein/RNA	52,444
Ligand/ion	196
Water	0
B-factors	102.4
Protein/RNA	102.5
Ligand/ion	59.3
Water	0
R.m.s. deviations	
Bond lengths (Å)	0.007
Bond angles (°)	1.23
PDB ID	4YY3

One crystal was used for the data set.
[a]Values in parentheses are for the highest resolution shell.
[b]Values were calculated by PHENIX.

crystal form, the tip of 16S rRNA helix 6 (known as the 30S subunit spur) from one 30S docks in the ribosomal P site of a second subunit, resembling a tRNA anticodon stem–loop (Fig. 3A). Additionally, the 3′-end of the 16S rRNA in this crystal form folds back into the mRNA tunnel and interacts with the spur to mimic an anticodon–codon interaction. As a result, it is impossible to bind any P-site ligands including mRNA in this crystal form. We attempted to soak into preformed 30S crystals combinations of wild-type HigB, a catalytic HigB variant (Hurley and Woychik 2009), wild-type mRNA (5′-AAAUAG-3′), and a noncleavable mRNA (5′-AAAUAG-3′) to program an AAA lysine codon in the A site and a UAG codon residing 3′ of the A site. In this mRNA fragment, the AAA lysine codon contains a 2′-methoxy modification that our laboratory showed prevents cleavage (Schureck et al. 2015). These approaches are similar to approaches previously used to observe 30S-bound ligands including IF1, 16S rRNA methyltransferase NpmA, and anticodon stem–loops of tRNAs bound to cognate and near-cognate codons of mRNAs (Carter et al. 2001; Ogle et al. 2001, 2002; Dunkle et al. 2014). Unbiased F_{obs}–F_{obs} electron difference density maps clearly show HigB bound in the A site (Fig. 2A,B; Supplemental Fig. S1), but no interpretable electron density was observed for the mRNA in all four HigB-mRNA soaks: wild-type HigB–wild-type mRNA; wild-type HigB–noncleavable mRNA; a catalytic HigB variant–wild-type mRNA; a catalytic HigB variant–noncleavable mRNA. The absence of mRNA in our structure is in contrast to all previous structures of the RelE, YoeB, and HigB toxins bound to the 70S ribosome (Neubauer et al. 2009; Feng et al. 2013; Schureck et al. 2015), in which the mRNA is pulled ∼9 Å from its normal path in the A site into the active site of the toxin (Fig. 3B). The lack of P-site tethering in the 30S crystal form, due to the 30S spur occupying the P site, may prevent the extreme rearrangement of the mRNA observed in 70S-toxin structures and possibly explains why mRNA was not observed in our 30S structure. Given that no other 30S-toxin structures exist, this seems possible. Thus, although this crystal structure does not provide any direct insights into how HigB interacts with the mRNA when bound to a 30S complex, it demonstrates that HigB can bind the ribosome in the absence of the mRNA, informs on key A-site interactions with HigB, and lastly, allows us to compare the 30S-HigB orientation with that of a 70S-HigB elongation complex (Schureck et al. 2015).

A-site bound HigB makes extensive interactions with ribosomal protein S12 and 16S rRNA helices h18, h30/31, h32, h34, and h44 (Fig. 2B–D). HigB is a small, compact protein (10.7 kDa) containing a single β-sheet surrounded by two flanking α-helices with a number of solvent-exposed, basic residues that likely play an important role in the recognition of the A-site environment. Like other ribosome-dependent toxins RelE and YoeB (Neubauer et al. 2009; Feng et al. 2013), HigB fits snugly in the A site, positioning a distinctive concave active site toward the mRNA path. Unlike interactions between tRNA and the A site, HigB makes a number of other interactions with five 16S rRNA helices likely to stabilize binding. Similar interactions of tRNAs with 16S rRNA may not be required for efficient binding because tRNAs bind to both the 30S and 50S subunits, with the chemical group attached to the tRNA 3′-end (e.g., deacylated, aminoacylated, or peptidyl) defining the ribosomal binding site preference (Lill et al. 1986; Schilling-Bartetzko et al. 1992). In contrast, HigB interacts exclusively with the small subunit and forms a network of hydrogen bonds and electrostatic interactions with the backbone of 16S rRNA helices that may aid in HigB recognizing the A site.

We next compared the 30S-HigB structure with that of *apo* 30S and 70S-HigB structures caught in precleavage and post-cleavage states (Wimberly et al. 2000; Schureck et al. 2015) (PDB codes 1J5E, 4YPB, and 4W4G). Comparison of the *apo* 30S and 30S-HigB structures reveals little to no changes indicating HigB does not induce large conformational rearrangement of the small subunit. HigB adopts an overall similar fold when bound to a 30S or 70S complex and binds in a nearly identical location in the A site (Fig. 2D). Interestingly, the relative location of the 30S head domain differs slightly

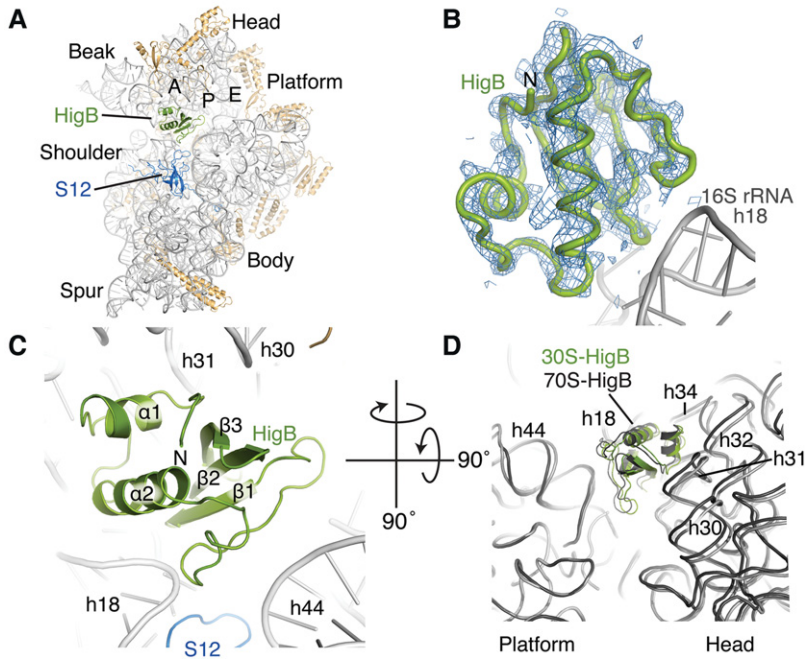

FIGURE 2. Structural insights into how HigB recognizes the 30S subunit. (*A*) The X-ray crystal structure of HigB bound to the A site of the 30S subunit. 16S rRNA and ribosomal proteins are shown in gray and tan, respectively, and the aminoacyl (A), peptidyl (P), exit (E) sites, and 30S domains are labeled. (*B*) Unbiased F_{obs}–F_{obs} difference electron density map of the 3.6 Å X-ray crystal structure of HigB bound to the *Thermus thermophilus* 30S subunit contoured to 1.5σ. F_{obs}–F_{obs} difference electron density map was calculated using the structure factors of the *apo* 30S structure (PDB code 1J5E). (*C*) Zoomed in view in the same orientation as in *A*, emphasizing how HigB interacts with multiple 16S rRNA helices and ribosomal protein S12. (*D*) Comparison of how HigB interacts with the 30S small subunit in the context of the 30S-HigB structure (green; this study) and 70S-HigB ΔH92 precleavage state structure (dark gray; PDB code 4YPB). The 16S rRNA body domain (nucleotides 560–912) of each structure was aligned by least-squares fit in the program Coot (Emsley et al. 2010). 16S rRNA nucleotides from the 30S-HigB and 70S-HigB structures are depicted in light gray and dark gray, respectively.

between the 30S- and 70S-bound forms of HigB. The 30S head domain is known to be flexible most prominently during the movement of mRNA and tRNA during translocation (Ratje et al. 2010; Guo and Noller 2012; Zhou et al. 2013). In the 30S-HigB structure, the 30S subunit adopts a more open head domain conformation (~3 Å) compared to the 70S–HigB complex (Schureck et al. 2015). One reason for these differences in domain closure may be the absence of P-site tRNA and the 50S. However, the fact that HigB can bind to two different conformations of the 30S head domain indicates there is flexibility in HigB–ribosome interactions, which may allow for recognition of different ribosome conformational states.

The A-site 16S rRNA nucleotides A1492, A1493, and G530 adopt different positions depending on the identity of the ligand bound at the A site. In the context of the 30S-HigB structure, A1492 and A1493 are located within h44 while G530 adopts a *syn* conformation, similar to the *apo* 30S structure (Wimberly et al. 2000). A 70S structure containing mRNA but no tRNA in the A site reveals that A1492 is partially extruded from h44 and A1493 is flipped from h44 (Jenner et al. 2010). In these two contexts, G530 also adopts the *syn* conformation. During decoding when tRNA engages the mRNA codon in the A site, 16S rRNA nucleotide C1054 packs beneath the third A-site nucleotide of the codon (Ogle et al. 2002). The A-site mRNA reorganization upon HigB binding to the 70S positions the Hoogsteen edge of the third A-site adenosine to base pair with the Watson–Crick face of C1054 (Schureck et al. 2015) (PDB code 4YPB). Comparison of these structures with the 30S-HigB-bound structures reveals no significant changes in the position of C1054. In summary, the binding of HigB to the ribosome, in the presence or absence of mRNA, causes little to no remodeling of the A site in contrast to when tRNA recognizes mRNA codons.

Two surface-exposed clusters of basic residues are required for HigB function

The HigB toxin has four surfaces that contact the ribosomal A-site 16S rRNA helices and S12 ribosomal protein (Fig. 2C).

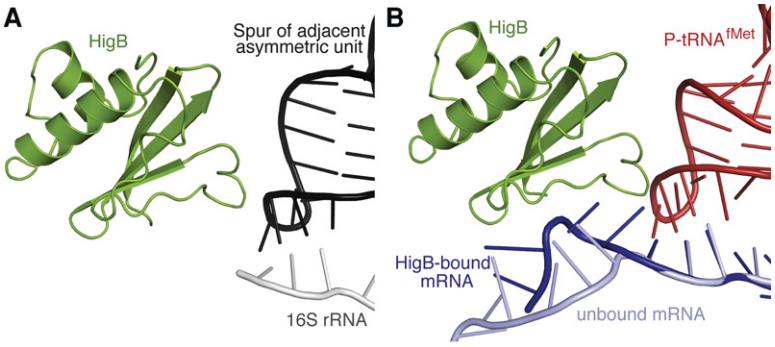

FIGURE 3. 30S crystal form likely prevents toxin-engaged mRNA in the A site. (*A*) In the context of the 30S crystal form, the 30S spur from a crystallographic symmetry mate packs in the P site and interacts with the 3′-end of the 16S rRNA, mimicking a P-site tRNA–mRNA pair. This arrangement only allows mRNA to be programmed starting at the A site in the 30S crystal form. (*B*) HigB binding to the ribosomal A site facilitates the mRNA being pulled into its active site in the context of a 70S-HigB ΔH92 complex in a precleavage state (PDB code 4YPB). The orientation that the mRNA adopts in the absence of toxin or tRNA is shown for comparison as light purple (PDB code 4V6G).

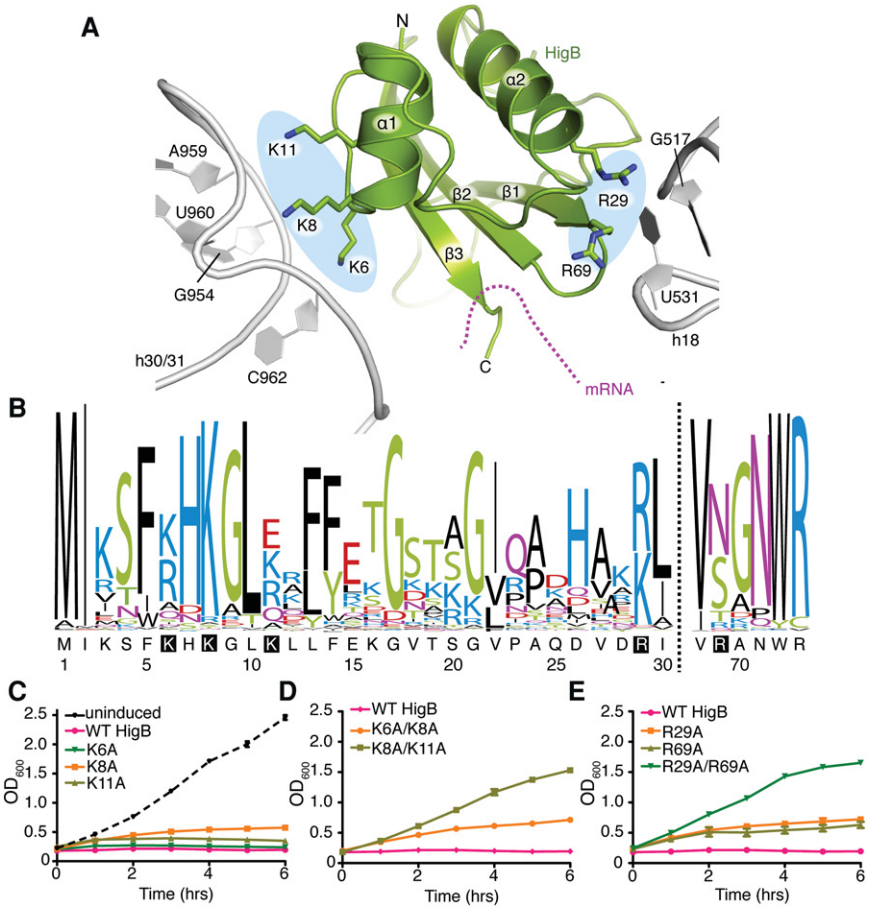

FIGURE 4. Two basic patches on the surface of HigB mediate recognition of 16S rRNA helices 18, 30, and 31. (*A*) HigB basic residues that interact with 16S rRNA cluster along two exposed surfaces (blue ovals) and are depicted as sticks. The mRNA path is shown as a dotted line as modeled from the 70S-HigB ΔH92 precleavage state (PDB code 4YPB) and is the location of the HigB active site. (*B*) Weblogo depiction of 1000 HigB homologs of the HigB regions (residues 1–30 and 68–73) that interact with 16S rRNA (Crooks et al. 2004). Residues are colored by the following scheme: Polar (G,S,T,Y,C; green), neutral (Q, N; magenta), basic (K, R, H; blue), acidic (D, E; red), and hydrophobic (A, V, L, I, P, W, F, M; black). *Proteus vulgaris* HigB residues are shown on the *x*-axis and residues that directly contact the 16S rRNA are depicted in white with black highlight. The *y*-axis indicates the bits with the height of the amino acid proportional to its frequency at that position. The total height of the stack is down-weighted if there is high variability while highly conserved positions are depicted as taller. (*C*) *E. coli* BW25113 growth assays show that overexpression of wild-type (WT) HigB halts cell growth (pink line) while uninduced HigB allows growth (black dash). HigB basic residues that directly interact with 16S rRNA were mutated to alanine and their effect on *E. coli* growth was monitored by optical density (OD) at 600 nm over 6 h. HigB patch one residues (K6, K8, and K11) were singly mutated and then doubly mutated in the sensitized K8A background (*D*). (*E*) HigB patch two residues (R29 and R69) were singly and in combination changed to alanine and their effect on *E. coli* growth was monitored at an OD at 600 nm over 6 h. For panels *B*–*D*, error bars display standard error of the mean from at least three experiments.

The first surface is closest to the ribosomal P site and includes three HigB lysine residues, K6, K8, and K11 (from α1) that form hydrogen bonds with the backbone of 16S rRNA head domain residues G954 (h30), U960–C962 and A959 (h31), respectively (Fig. 4A). Among ~1000 HigB homologs, K8 is the most conserved residue of the three lysines (Fig. 4B). At position six, HigB contains charged residues (lysine or arginine), and at residue position eleven there can be a number of different types of residues (glutamic acid, lysine, arginine, glutamine). Adjacent to the first surface are the side chains of HigB loop 2 residues T19 and Q25 and the carbonyl of S20 that interact with C1214, U531, and G1050 (h18), respectively. On the opposite side of the first HigB surface are residues R29 (from α2) and R69 (from β1) that likely form electrostatic interactions with G517 and U531 (h18), respectively. A lysine or arginine is found at HigB residue 29 but in the case of residue 69, a positively charged residue is not highly conserved and a diversity of residues exists (asparagine, serine, threonine, arginine) (Fig. 4B). Lastly, HigB residue Q49 interacts with ribosomal protein S12 residues T44 and S50. The structures of RelE and YoeB bound to the 70S reveal that each contacts similar regions of the A site and two patches of basic residues that contact h30/h31 and h18 of the head domain are common features among all three (Fig. 5).

To examine the role these basic residues play in HigB function, we monitored bacterial growth upon overexpression of HigB proteins altered in these regions. Overexpression of wild-type HigB in *E. coli* causes growth inhibition and mutation of residues essential for HigB toxicity relieves the growth suppression (Tian et al. 1996; Hurley and Woychik 2009). We used this assay to determine whether HigB residue changes that directly interact with 16S rRNA confer HigB toxicity (i.e., cell growth inhibition) or normal cell growth, with the latter being the inability of HigB to bind the ribosome similar to what was seen for the YafQ toxin (Maehigashi et al. 2015). Single alanine substitutions of HigB residues K6 and K11 result in HigB variants that retain the ability to suppress bacterial growth while the mutation of K8 shows a slight alleviation of the growth defect (Fig. 4C). Thus, it appears each of these three lysine residues is not individually critical for HigB function. The HigB K6A/K8A variant also slightly relieves growth suppression, similarly to the K8A single variant, while the K8A/K11A double variant allows for normal growth (Fig. 4D). This latter result suggests HigB function is ablated upon substitution of both K8 and K11 and that the K8/K11 and 16S rRNA h31 nucleotides A959–C962

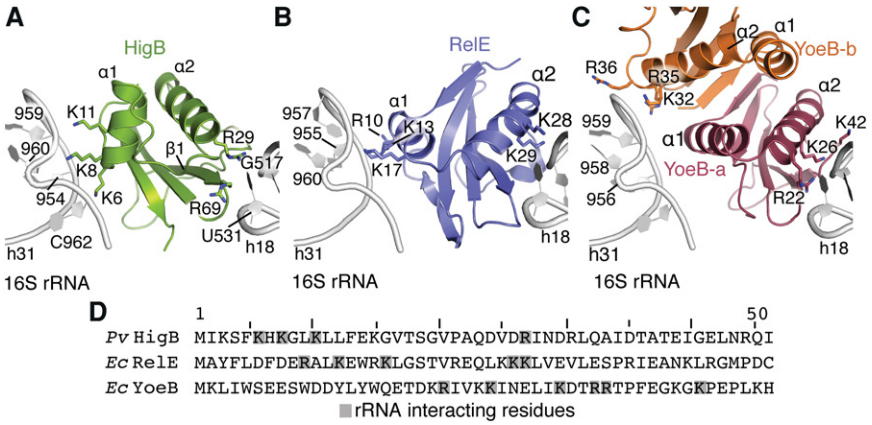

FIGURE 5. Ribosome-dependent toxins recognize the head domain of the 30S subunit. Views of HigB (*A*; this study), RelE (*B*; PDB code 4V7J), and YoeB (*C*; PDB code 4V8X) interacting with h18 and h31 rRNA via basic residues. The RelE and YoeB structures were captured in the precleavage state and basic residues within hydrogen bonding distance of h18 and h31 are shown as sticks. (*D*) Alignment of regions of ribosome-dependent toxins *Proteus vulgaris (Pv)* HigB, *E. coli (Ec)* RelE, and *E. coli (Ec)* YoeB that interact with 16S rRNA, demonstrating the low sequence identities.

interactions are likely critical for HigB recognition of the ribosomal A site.

One possibility in these assays is that the introduction of HigB point variants alters the overall tertiary fold thus rendering HigB insoluble. This outcome would lead to the restoration of normal bacterial growth suggesting erroneously that the residues play a key role in HigB function. Therefore, to confirm that each HigB variant was expressed and soluble, we examined the expression of HigB variants after 4 h post induction by Western blot analysis using polyclonal antibodies against the HigBA complex (Supplemental Fig. S2). We show that *E. coli* harboring wild-type HigB does not result in a detectable signal in the immunoblot indicative of the toxin causing an overall inhibition of protein synthesis as seen with other toxins such as MqsR (Supplemental Fig. S2, lane 3; Brown et al. 2009). The single point variants K6A and K11A show the absence of HigB (Supplemental Fig. S2, lanes 4 and 6) suggesting these HigB variants are still active. Indeed, this conclusion is also consistent with their ability to suppress bacterial growth (Fig. 4C). HigB K8A and K6A/K8A variants slightly relieve the inhibition of bacterial growth (Fig. 4C,D) with Western blot analysis demonstrating the protein variants are expressed (Supplemental Fig. S2, lanes 5 and 9). These results suggest that HigB K8A and K6A/K8A variants have a decrease in binding to the 30S, which, in turn, prevents HigB toxicity and allows for HigB K8A and K6A/K8A protein expression. The interpretation of the HigB K8A/K11A variant results is more complex in that although bacterial growth is fully restored indicating this HigB variant is inactive (Fig. 4D), Western blot analysis indicates lower protein expression (Supplemental Fig. S2, lane 10). Therefore, one interpretation could be that these changes to HigB affect its solubility thus appearing to relieve the bacterial growth suppression phenotype. Since it is known that bacterial growth inhibition can be caused by extremely low toxin protein expression levels (Overgaard et al. 2008; Brown et al. 2009) (and our wild-type HigB overexpression bacterial growth assays; Supplemental Fig. S2, lane 3), the fact that the K8A/K11A variant is even detectable by immunoblot argues that the HigB K8A/K11A variant is not fully active.

The importance of the other two solvent-exposed HigB residues R29 and R69 was similarly tested. HigB proteins carrying single point variants R29A and R69A display an intermediate growth suppression phenotype, whereas a double R29A/R69A variant inactivated HigB, allowing for normal growth (Fig. 4E). Although in all three cases there are robust signals for HigB expression (Supplemental Fig. S2, lanes 7, 8, and 11), these HigB variants are defective in binding the ribosome, which reduces their impact on bacterial growth and toxicity. Together, these data provide support that HigB uses both patches of basic residues to probe the contours of the A-site rRNA along similar lines to how toxin YafQ recognizes the ribosome (Maehigashi et al. 2015).

DISCUSSION

Our biochemical and structural analyses demonstrate that the ribosome-dependent *P. vulgaris* HigB toxin productively recognizes the 30S subunit suggesting an initiation complex may be an in vivo target. HigB is positioned in the ribosomal A site and uses two solvent exposed basic patches of lysine and arginine residues to recognize the 16S rRNA backbone. We further show that mutating these clusters of residues in combination (K8A/K11A or R29A/R69A) impacts HigB activity and thus toxicity, allowing for bacterial growth (Fig. 4). Comparison with another ribosome-dependent toxin *E. coli* RelE reveals two equivalent clusters of solvent-exposed residues that interact with the ribosome albeit derived from distinct secondary structural elements (Fig. 5B; Neubauer et al. 2009). Although RelE and HigB are structural homologs (rmsd 2.2 Å; PDB codes 4FXE and 4MCT) containing a core β-sheet flanked by 2 or 3 α-helices, these toxins have no sequence conservation among residues that contact the ribosome (Fig. 5D). RelE residues R10, K13, and K17 emanate from α1 to contact h31 similar to HigB α1 although the helices differ in their orientation by ~90° (Fig. 5A,B). In contrast, RelE residues K28 and K29 from α2 interact with h18 while HigB residues R29 and R69 from the tips of α2 and β1, respectively, protrude to recognize h18. Despite the differences in the modes of 16S rRNA recognition, common features of the RelE and HigB remain intact and suggest a

conserved binding mechanism for ribosome-dependent mRNA endonucleases.

Ribosome-dependent toxin *E. coli* YoeB also adopts the same microbial RNase core fold of RelE and HigB, but differs considerably in its interactions with the ribosomal A site (Fig. 5C; Feng et al. 2013). First, YoeB forms a dimer off and on the ribosome, a state that alters how it interacts with 16S rRNA (Kamada and Hanaoka 2005; Feng et al. 2013). The YoeB protomer that interacts with mRNA (called YoeB-a) has a similar α-helix (α2) positioned to form interactions with 16S rRNA h18. However, the interaction between YoeB-a α1 and 16S rRNA h31, which is present in HigB and RelE, is nonexistent likely because of the dimer interface. Instead, the second protomer of YoeB (YoeB-b) interacts more distantly on h31 with nucleotides U956, A958, and A959. Recent studies demonstrate that YoeB is activated during thermal stress (Janssen et al. 2015); this temperature dependence may be an underlying reason for YoeB adopting a dimeric form presumably to provide thermal stability but this is not currently understood.

Toxin abundance and accessibility of the A site likely both play important roles in determining optimal mRNA substrate selection and activity by ribosome-dependent toxins. Since toxins are expressed at low levels during both non-stress and stress environmental conditions (Overgaard et al. 2008; Li et al. 2014), and bind within the same range of affinities as tRNAs (Maehigashi et al. 2015), an argument could be made that the most important determinant for their activity is the accessibility of the A-site mRNA. A preference for cleaving mRNAs during initiation or termination of translation would allow toxins greater access to the A-site mRNA given that each of these steps in translation is slow and, in the case of initiation, is the rate-limiting step of protein synthesis. Indeed, a number of toxins appear to target these two ribosomal states. Although RelE can efficiently cleave sense codons (Hurley et al. 2011), stop codons are also targeted (Pedersen et al. 2003). Moreover, YoeB cleaves at codons following the AUG start codon in addition to at the UAA stop codon (Christensen et al. 2004; Christensen-Dalsgaard and Gerdes 2008; Zhang and Inouye 2009). YafQ has been shown to only cleave the AAA lysine codon while AAA is a preferred HigB target. This codon is the most abundant after the start codon in certain bacteria (Hurley and Woychik 2009; Prysak et al. 2009). Exploitation of the slowest steps in translation by ribosome-dependent toxins may have evolved to limit competition with highly abundant molecules like tRNAs or translation factors. Our results show that the 30S initiation-competent complex is a substrate for HigB similar to what was previously observed for the RelE toxin (Pedersen et al. 2003). Additionally, since ribosome profiling experiments show that ribosomes spend a large amount of time at the beginning of transcripts (Oh et al. 2011), this may provide toxins like YafQ, YoeB, or HigB an advantage in accessing their substrates.

If the bacterial initiation step of translation is a target for HigB, one question is, when during initiation? Initiation is a multistep, kinetically controlled process whereby initiation factors IF1, IF2, and IF3 along with mRNA and fMet-tRNA^{fMet} form a 30S initiation complex (Schmeing and Ramakrishnan 2009). Hydrolysis of GTP by IF2 signals the dissociation of factors before subunit association with the 50S. Comparison of IF1 bound to the 30S to the 30S-HigB structure indicates significant steric clash between HigB α2, loop 3, β1, loop 4, and β2 and IF1 (Fig. 6A). This overlap suggests HigB would have access to the 30S A site only after IF1 dissociation. Since both the 30S initiation-competent and the 70S initiation complexes are targeted by HigB (this study and Schureck et al. 2015) and ribosomes spend a large amount of time at the initiation stage (Oh et al. 2011), both states present equally good opportunities to cleave ribosome-bound mRNA to alter the translational landscape during stress.

Translation initiation is rate-limiting and the slowest step of protein synthesis presenting an ideal situation for a toxin to target mRNA for cleavage. However, ribosome-dependent toxins RelE, HigB, YoeB, and YafQ have overlapping binding sites with IF1 indicating they likely do not bind in the A site while IF1 is present (Fig. 6B,C). The YafO toxin requires the ribosome for mRNA cleavage similar to the HigB, RelE, YoeB, and YafQ toxins (Zhang et al. 2009; Christensen-Dalsgaard et al. 2010), yet does not cleave mRNAs in the A site of the ribosome and instead cleaves ~8-nt downstream from the A-site codon near the mRNA entrance tunnel (Zhang et al. 2009). Thus, in contrast to other ribosome-dependent toxins, YafO-mediated mRNA cleavage would not be inhibited by the presence of IF1 likely allowing YafO to

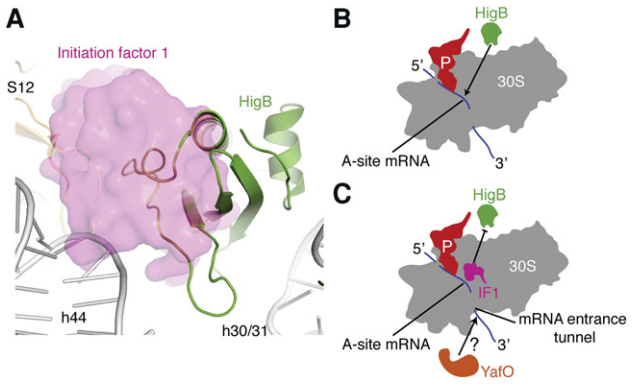

FIGURE 6. Model for toxin recognition of the ribosome. (*A*) Overlay of Initiation factor 1 (IF1, pink) and HigB (green) bound to 30S subunit. The IF1 protein is shown as a surface representation to highlight the extensive overlap between HigB and IF1. The 30S-IF1 structure (PDB code 1HR0) was aligned to the 30-HigB structure by least-squares fitting of 16S rRNA. (*B*) HigB can target a 30S initiation-competent complex but not in the presence of IF1. (*C*) The YafO toxin cleaves mRNA at the downstream mRNA entrance tunnel and not in the A site as other ribosome-dependent toxins in contrast to HigB, YafQ, YoeB, and RelE and during the translation cycle.

cleave mRNA during the initiation process even in the presence of IF1 but also at any point along the entire translation cycle (Fig. 6C). Taken together, it appears bacteria have multiple mechanisms to inhibit translation initiation during stress.

MATERIALS AND METHODS

Strains and plasmids

E. coli BW25113 [Δ(*araD-araB*)*567* Δ(*rhaD-rhaB*)*568* Δ*lacZ4787* (::rrnB-3) *hsdR514 rph-1*] were used for all bacterial growth assays and to express wild-type HigB(His)$_6$ (Datsenko and Wanner 2000). Plasmids pBAD24-HigB and pBAD-Myc-HisA-HigB(His)$_6$ were kind gifts from Professor Nancy A. Woychik (Rutgers University). All single amino acid changes were introduced by site-directed mutagenesis and sequences were verified by DNA sequencing (Genewiz).

Purification of *E. coli* 30S ribosomes

E. coli 30S ribosomes were similarly purified as described previously (Powers and Noller 1991). *E. coli* MRE600 cells were grown in Lysogeny Broth (LB) to an optical density (OD) at 600 nm of 0.7 at 37°C followed by incubation on ice for 20 min. Cells were pelleted (all centrifugation steps carried out at 4°C), washed in buffer 1 (10 mM HEPES/KOH pH 7.6, 10 mM $MgCl_2$, 1 M NH_4Cl, and 6 mM β-mercaptoethanol [β-Me]), and resuspended in buffer 2 (same as buffer 1 except with NH_4Cl reduced to 100 mM). Cells were lysed using a high-pressure homogenizer (Emulsiflex), cell debris was pelleted for 10 min at 17,000*g* and the supernatant containing ribosomes was further centrifuged for 3 h at 274,000*g*. The pelleted ribosomes were resuspended in 4 mL buffer 2 and dialyzed against 10 mM HEPES/KOH pH 7.6, 0.3 mM $MgCl_2$, 100 mM NH_4Cl, and 6 mM β-Me to separate the subunits. This solution was applied to a 10%–30% linear sucrose gradient, centrifuged overnight at 23,000 rpm in a Beckman SW28 rotor, and the 30S and 50S subunits fractionated. The 30S fractions were pooled, buffer adjusted to 10 mM $MgCl_2$, concentrated by pelleting through a 1.2 M sucrose cushion at 274,000*g*, resuspended in buffer 2, flash-frozen in liquid nitrogen and stored at −80°C.

HigB expression and purification

A culture of *E. coli* BW25113 cells harboring pBAD-Myc-HisA-HigB (His)$_6$ was grown overnight at 37°C in M9 minimal medium supplemented with 0.2% w/v casamino acids, 100 µg/mL ampicillin, and 0.2% (w/v) glucose. A 1:100 dilution was used to inoculate 1 L of fresh M9 medium supplemented with 0.21% (w/v) glycerol, and the culture was grown until an OD at 600 nm of 0.7 was reached. Protein expression was induced with 0.04% (w/v) arabinose and the culture was grown for an additional 3 h before harvesting by centrifugation at 3,500*g* and stored at −20°C. Thawed cell pellets from 1 L cultures were resuspended in 35 mL lysis buffer (20 mM Tris–HCl, pH 7.5, 10% [w/v] glycerol, 250 mM KCl, 5 mM $MgCl_2$, 5 mM β-Me, 0.2 mM phenylmethylsulfonyl fluoride, and 0.1% [w/v] Triton X-100) and lysed by sonication. Cell debris was removed by centrifugation for 45 min at 39,000*g*. The supernatant was passed through a 0.45 µM filter before loading onto a 1 mL Ni^{2+}-nitrilotriacetic acid column attached to an ÄKTApurifier10 (GE Healthcare) at 10°C. The column was washed with 25 column volumes of loading buffer (40 mM Tris–HCl, pH 7.5, 10% [w/v] glycerol, 250 mM KCl, 5 mM $MgCl_2$, 5 mM β-Me, and 20 mM imidazole) and protein was eluted with a linear 25 CV gradient of loading buffer containing 500 mM imidazole. Fractions containing HigB protein were concentrated in a 3000 molecular weight cut off (MWCO) concentrator (Millipore), filtered through a 0.45 µM Spin-X filter (Corning) and loaded onto a Superdex S75 10/300 column (GE Healthcare) preequilibrated in sizing buffer (40 mM Tris–HCl, pH 7.5, 250 mM KCl, 5 mM $MgCl_2$, and 5 mM β-Me). Fractions containing HigB judged to be over 95% pure by SDS-PAGE were pooled, concentrated to 10 µM, flash frozen in liquid nitrogen, and stored at −80°C.

mRNA cleavage assays

A final concentration of 1.2 µM *E. coli* 30S was incubated with 0.6 µM 5′-^{32}P-labeled mRNA (5′-GGCAAGGAGGUAAAAAUGAAA UAGU-3′; ThermoFisher) at 37°C for 6 min followed by incubation with 3 µM *E. coli* tRNA^{fMet} (Chemical Block) for 30 min at 37°C. Reactions were initiated by the addition of 0.9 µM HigB, and aliquots were removed at 1, 3, 10, 30, and 60 min, and quenched by the addition of 2× formamide dye (98% formamide, 10 mM EDTA, pH 8.0 and 0.2 mg mL^{-1} bromophenol blue) followed by heating at 70°C for 2 min. The reactions were run on a denaturing 8 M urea, 18% polyacrylamide gel where the mRNA substrate was separated from cleavage products. The gel was fixed, dried, and visualized by exposure to a phosphor screen followed by imaging on a Typhoon FLA 7000 gel imager (GE Healthcare).

Structure determination of the 30S-HigB complex

Thermus thermophilus 30S ribosomes were purified, crystallized, and cryoprotected as described previously (Clemons et al. 2001). Before soaking into the 30S crystals, HigB was equilibrated into the ribosome buffer (5 mM HEPES pH 7.5, 50 mM KCl, 10 mM NH_4Cl, and 10 mM MgOAc) via dilution followed by concentration in a 3000 MWCO concentrator. A solution containing a final concentration of 175 µM HigB and 700 µM mRNA (5′-AmAmAm UAG-3′ where "m" indicates a 2′-OCH_3 modification to prevent cleavage) was incubated with the *apo* 30S crystals for 24 h. Crystals were flash frozen in liquid nitrogen and data collection performed at the Northeast Regional Access Team (NE-CAT) 24-IDE beamline. X-ray diffraction images were collected at a wavelength of 0.979 Å using 0.2° oscillations for 36°. Data were integrated and scaled using XDS (Kabsch 2010), the test set of reflections was inherited from a previously solved structure of the *apo* 30S (PDB code 1J5E) (Wimberly et al. 2000), and a 30S model lacking the NpmA protein (PDB code 4OX9) (Dunkle et al. 2014) was used as a starting model for refinement in PHENIX (Adams et al. 2010). The initial refinement of the 30S coordinates lacking HigB or mRNA produced unbiased $F_{obs}-F_{obs}$ difference electron density with a clear signal for HigB. Unbiased $F_{obs}-F_{obs}$ difference electron density maps were generated in PHENIX using the *apo* 30S structure (PDB code 1J5E), which is isomorphous with the 30S-HigB structure (cell dimensions vary by 0.375%). The 1.25 Å structure of HigB (residues 1–89) (PDB code 4PX8) (Schureck et al. 2015) was placed into

the difference electron density in Coot and rebuilt (Emsley et al. 2010). After remodeling of A-site rRNA, rRNA flanking the remodeled regions was individually refined while all other rRNA, ribosomal proteins, and HigB were refined as rigid groups in PHENIX. The 30S-HigB structure was refined to a final R_{work}/R_{free} of 21.4/23.9%.

Bacterial growth assays

Monitoring of bacterial growth upon overexpression of wild-type and HigB variants was performed as previously described (Hurley and Woychik 2009). *E. coli* BW251113 carrying pBAD24 vectors encoding either wild-type or HigB variants were grown in M9 minimal medium supplemented with 0.2% w/v casamino acids, 100 µg/mL ampicillin and either glucose (0.2% w/v) for overnight cultures, or glycerol (0.21% w/v) for protein overexpression assays. Cultures were inoculated with a 1:100 dilution of an overnight culture, shaken at 250 rpm at 37°C and induced with 0.2% (w/v) arabinose at an OD at 600 nm of 0.2. Growth was monitored every hour for 6 h after induction, and the average OD_{600} values along with the standard error of the mean (SEM) were plotted in GraphPad Prism 5. Soluble HigB protein from the growth assays was assayed at 4 h post induction by Western blot analysis with primary polyclonal antibodies against the HigBA complex (kind gift from Professor Nancy A. Woychik, Rutgers University). Cells were lysed by sonication, cell debris was cleared by centrifugation, and the supernatant fractions containing soluble protein were analyzed on SDS-PAGE gels. The soluble fraction from equal numbers of cells was separated on a 4%–20% denaturing SDS-PAGE gel (Bio-Rad) and anti-rabbit IgG (Sigma) and the ECL-prime kit (GE Healthcare) was used for chemiluminescent detection. Recombinant HigBA was used as control and was expressed and purified as previously described (Schureck et al. 2014).

DATA DEPOSITION

Crystallography, atomic coordinates, and structure factors have been deposited in the Protein Data Bank, www.pdb.org (PDB code 4YY3).

SUPPLEMENTAL MATERIAL

Supplemental material is available for this article.

ACKNOWLEDGMENTS

Research reported in this publication was partially supported by a National Science Foundation CAREER award, Division of Molecular and Cellular Biosciences 0953714 (C.M.D.), National Institutes of Health (NIH) GM093278 (C.M.D.), a NIH Biochemistry, Cellular and Molecular Biology (BCMB) Graduate Training Grant 5T32GM8367 (M.A.S.), and NIH National Research Service Award F31 Fellowship GM108351 (M.A.S.). C.M.D. is a Pew Scholar in the Biomedical Sciences. We thank Dunham laboratory members J.A. Dunkle, C.E. Fagan, and E.A. Hoffer for help in data collection, data analysis, and figure production. We also thank Dr. G.L. Conn for critical reading of the manuscript. This work is based on research conducted at the APS on the NE-CAT ID24-E beamline, which is supported by National Institute of General Medical Sciences from the National Institutes of Health (P41 GM103403), and at the SER-CAT beamline. Use of the APS, an Office of Science User Facility operated for the US DOE Office of Science by ANL, was supported under Contract DE-AC02-06CH11357.

Received February 15, 2016; accepted May 7, 2016.

REFERENCES

Adams PD, Afonine PV, Bunkóczi G, Chen VB, Davis IW, Echols N, Headd JJ, Hung LW, Kapral GJ, Grosse-Kunstleve RW, et al. 2010. PHENIX: a comprehensive Python-based system for macromolecular structure solution. *Acta Crystallogr* **66:** 213–221.

Boutte CC, Crosson S. 2013. Bacterial lifestyle shapes stringent response activation. *Trends Microbiol* **21:** 174–180.

Brown BL, Grigoriu S, Kim Y, Arruda JM, Davenport A, Wood TK, Peti W, Page R. 2009. Three dimensional structure of the MqsR: MqsA complex: a novel TA pair comprised of a toxin homologous to RelE and an antitoxin with unique properties. *PLoS Pathog* **5:** e1000706.

Carter AP, Clemons WM Jr, Brodersen DE, Morgan-Warren RJ, Hartsch T, Wimberly BT, Ramakrishnan V. 2001. Crystal structure of an initiation factor bound to the 30S ribosomal subunit. *Science* **291:** 498–501.

Christensen-Dalsgaard M, Gerdes K. 2008. Translation affects YoeB and MazF messenger RNA interferase activities by different mechanisms. *Nucleic Acids Res* **36:** 6472–6481.

Christensen SK, Maenhaut-Michel G, Mine N, Gottesman S, Gerdes K, Van Melderen L. 2004. Overproduction of the Lon protease triggers inhibition of translation in Escherichia coli: involvement of the *yefM-yoeB* toxin-antitoxin system. *Mol Microbiol* **51:** 1705–1717.

Christensen-Dalsgaard M, Jorgensen MG, Gerdes K. 2010. Three new RelE-homologous mRNA interferases of *Escherichia coli* differentially induced by environmental stresses. *Mol Microbiol* **75:** 333–348.

Clemons WM Jr, Brodersen DE, McCutcheon JP, May JL, Carter AP, Morgan-Warren RJ, Wimberly BT, Ramakrishnan V. 2001. Crystal structure of the 30 S ribosomal subunit from *Thermus thermophilus*: purification, crystallization and structure determination. *J Mol Biol* **310:** 827–843.

Crooks GE, Hon G, Chandonia JM, Brenner SE. 2004. WebLogo: a sequence logo generator. *Genome Res* **14:** 1188–1190.

Datsenko KA, Wanner BL. 2000. One-step inactivation of chromosomal genes in *Escherichia coli* K-12 using PCR products. *Proc Natl Acad Sci* **97:** 6640–6645.

Dunkle JA, Vinal K, Desai PM, Zelinskaya N, Savic M, West DM, Conn GL, Dunham CM. 2014. Molecular recognition and modification of the 30S ribosome by the aminoglycoside-resistance methyltransferase NpmA. *Proc Natl Acad Sci* **111:** 6275–6280.

Emsley P, Lohkamp B, Scott WG, Cowtan K. 2010. Features and development of Coot. *Acta Crystallogr* **66:** 486–501.

Feng S, Chen Y, Kamada K, Wang H, Tang K, Wang M, Gao YG. 2013. YoeB-ribosome structure: a canonical RNase that requires the ribosome for its specific activity. *Nucleic Acids Res* **41:** 9549–9556.

Gerdes K, Christensen SK, Lobner-Olesen A. 2005. Prokaryotic toxin-antitoxin stress response loci. *Nat Rev Microbiol* **3:** 371–382.

Guo Z, Noller HF. 2012. Rotation of the head of the 30S ribosomal subunit during mRNA translocation. *Proc Natl Acad Sci* **109:** 20391–20394.

Hurley JM, Woychik NA. 2009. Bacterial toxin HigB associates with ribosomes and mediates translation-dependent mRNA cleavage at A-rich sites. *J Biol Chem* **284:** 18605–18613.

Hurley JM, Cruz JW, Ouyang M, Woychik NA. 2011. Bacterial toxin RelE mediates frequent codon-independent mRNA cleavage from the 5′ end of coding regions in vivo. *J Biol Chem* **286:** 14770–14778.

Janssen BD, Garza-Sanchez F, Hayes CS. 2015. YoeB toxin is activated during thermal stress. *Microbiologyopen* **4:** 682–697.

Jenner L, Demeshkina N, Yusupova G, Yusupov M. 2010. Structural rearrangements of the ribosome at the tRNA proofreading step. *Nat Struct Mol Biol* **17:** 1072–1078.

Kabsch W. 2010. Xds. *Acta Crystallogr* **66:** 125–132.

Kamada K, Hanaoka F. 2005. Conformational change in the catalytic site of the ribonuclease YoeB toxin by YefM antitoxin. *Mol Cell* **19:** 497–509.

Li GW, Burkhardt D, Gross C, Weissman JS. 2014. Quantifying absolute protein synthesis rates reveals principles underlying allocation of cellular resources. *Cell* **157:** 624–635.

Lill R, Robertson JM, Wintermeyer W. 1986. Affinities of tRNA binding sites of ribosomes from *Escherichia coli*. *Biochemistry* **25:** 3245–3255.

Loris R, Garcia-Pino A. 2014. Disorder- and dynamics-based regulatory mechanisms in toxin-antitoxin modules. *Chem Rev* **114:** 6933–6947.

Maehigashi T, Ruangprasert A, Miles SJ, Dunham CM. 2015. Molecular basis of ribosome recognition and mRNA hydrolysis by the *E. coli* YafQ toxin. *Nucleic Acids Res* **43:** 8002–8012.

Maisonneuve E, Gerdes K. 2014. Molecular mechanisms underlying bacterial persisters. *Cell* **157:** 539–548.

Neubauer C, Gao YG, Andersen KR, Dunham CM, Kelley AC, Hentschel J, Gerdes K, Ramakrishnan V, Brodersen DE. 2009. The structural basis for mRNA recognition and cleavage by the ribosome-dependent endonuclease RelE. *Cell* **139:** 1084–1095.

Ogle JM, Brodersen DE, Clemons WM Jr, Tarry MJ, Carter AP, Ramakrishnan V. 2001. Recognition of cognate transfer RNA by the 30S ribosomal subunit. *Science* **292:** 897–902.

Ogle JM, Murphy FV, Tarry MJ, Ramakrishnan V. 2002. Selection of tRNA by the ribosome requires a transition from an open to a closed form. *Cell* **111:** 721–732.

Oh E, Becker AH, Sandikci A, Huber D, Chaba R, Gloge F, Nichols RJ, Typas A, Gross CA, Kramer G, et al. 2011. Selective ribosome profiling reveals the cotranslational chaperone action of trigger factor in vivo. *Cell* **147:** 1295–1308.

Overgaard M, Borch J, Jorgensen MG, Gerdes K. 2008. Messenger RNA interferase RelE controls relBE transcription by conditional cooperativity. *Mol Microbiol* **69:** 841–857.

Pandey DP, Gerdes K. 2005. Toxin-antitoxin loci are highly abundant in free-living but lost from host-associated prokaryotes. *Nucleic Acids Res* **33:** 966–976.

Pedersen K, Zavialov AV, Pavlov MY, Elf J, Gerdes K, Ehrenberg M. 2003. The bacterial toxin RelE displays codon-specific cleavage of mRNAs in the ribosomal A site. *Cell* **112:** 131–140.

Powers T, Noller HF. 1991. A functional pseudoknot in 16S ribosomal RNA. *EMBO J* **10:** 2203–2214.

Prysak MH, Mozdzierz CJ, Cook AM, Zhu L, Zhang Y, Inouye M, Woychik NA. 2009. Bacterial toxin YafQ is an endoribonuclease that associates with the ribosome and blocks translation elongation through sequence-specific and frame-dependent mRNA cleavage. *Mol Microbiol* **71:** 1071–1087.

Ratje AH, Loerke J, Mikolajka A, Brunner M, Hildebrand PW, Starosta AL, Donhofer A, Connell SR, Fucini P, Mielke T, et al. 2010. Head swivel on the ribosome facilitates translocation by means of intra-subunit tRNA hybrid sites. *Nature* **468:** 713–716.

Sato T, Terabe M, Watanabe H, Gojobori T, Hori-Takemoto C, Miura K. 2001. Codon and base biases after the initiation codon of the open reading frames in the *Escherichia coli* genome and their influence on the translation efficiency. *J Biochem* **129:** 851–860.

Schilling-Bartetzko S, Franceschi F, Sternbach H, Nierhaus KH. 1992. Apparent association constants of tRNAs for the ribosomal A, P, and E sites. *J Biol Chem* **267:** 4693–4702.

Schmeing TM, Ramakrishnan V. 2009. What recent ribosome structures have revealed about the mechanism of translation. *Nature* **461:** 1234–1242.

Schureck MA, Maehigashi T, Miles SJ, Marquez J, Cho SE, Erdman R, Dunham CM. 2014. Structure of the *Proteus vulgaris* HigB-(HigA)2-HigB toxin-antitoxin complex. *J Biol Chem* **289:** 1060–1070.

Schureck MA, Dunkle JA, Maehigashi T, Miles SJ, Dunham CM. 2015. Defining the mRNA recognition signature of a bacterial toxin protein. *Proc Natl Acad Sci* **112:** 13862–13867.

Tian QB, Ohnishi M, Tabuchi A, Terawaki Y. 1996. A new plasmid-encoded proteic killer gene system: cloning, sequencing, and analyzing hig locus of plasmid Rts1. *Biochem Biophys Res Commun* **220:** 280–284.

Wimberly BT, Brodersen DE, Clemons WM Jr, Morgan-Warren RJ, Carter AP, Vonrhein C, Hartsch T, Ramakrishnan V. 2000. Structure of the 30S ribosomal subunit. *Nature* **407:** 327–339.

Yamaguchi Y, Inouye M. 2011. Regulation of growth and death in *Escherichia coli* by toxin-antitoxin systems. *Nat Rev Microbiol* **9:** 779–790.

Zhang Y, Inouye M. 2009. The inhibitory mechanism of protein synthesis by YoeB, an *Escherichia coli* toxin. *J Biol Chem* **284:** 6627–6638.

Zhang Y, Yamaguchi Y, Inouye M. 2009. Characterization of YafO, an *Escherichia coli* toxin. *J Biol Chem* **284:** 25522–25531.

Zhou J, Lancaster L, Donohue JP, Noller HF. 2013. Crystal structures of EF-G-ribosome complexes trapped in intermediate states of translocation. *Science* **340:** 1236086.

mRNA bound to the 30S subunit is a HigB toxin substrate

Marc A. Schureck, Tatsuya Maehigashi, Stacey J. Miles, et al.

RNA 2016 22: 1261-1270 originally published online June 15, 2016
Access the most recent version at doi:10.1261/rna.056218.116